Polymer 53 (2012) 5469–5475

Contents lists available at SciVerse ScienceDirect

Polymer

journal homepage: www.elsevier.com/locate/polymer

Microfluidic synthesis of macroporous polymer immunobeads

Kunqiang Jiang [a], Alex Sposito [b], Jikun Liu [b], Srinivasa R. Raghavan [c,**], Don L. DeVoe [b,*]

[a] Department of Chemistry & Biochemistry, University of Maryland, College Park, MD 20742, USA
[b] Department of Mechanical Engineering, University of Maryland, College Park, MD 20742, USA
[c] Department of Chemical & Biomolecular Engineering, University of Maryland, College Park, MD 20742, USA

ARTICLE INFO

Article history:
Received 11 July 2012
Received in revised form
28 September 2012
Accepted 29 September 2012
Available online 5 October 2012

Keywords:
Microbeads
Monoliths
Immunocapture

ABSTRACT

This article describes the synthesis and characterization of a new type of discrete microparticle immunosensor employing macroporous methacrylate polymer microspheres. The microspheres are produced using a simple microfluidic tubing co-flow droplet generator to produce large populations of microparticles with exceptional size uniformity and controllable macroporosity. Subsequent grafting treatments are demonstrated to anchor immunoactive ligands on the porous surfaces, converting the microspheres into discrete immunosensor elements, with direct immunoassay tests demonstrating good detection limits and capturing specificity. This work demonstrates the adaptation of a traditional polymer monolith stationary phase material into a discrete microparticle immunosensor format using a synthesis and functionalization path with significant flexibility toward a diverse range of biological and chemical sensing applications.

1. Introduction

Macroporous polymers, whose internal structures can be tailored to exhibit pores with dimensions ranging from hundreds of nanometers to several micrometers, are widely used as stationary phases in chromatography and solid supports in affinity extraction [1–8]. Macroporous polymers offer outstanding mass transfer efficiency, low hydrodynamic resistance, and simple and versatile surface modifications [1–7,10,11]. Macroporous polymer supports are widely available in various geometries, including disks, columns, tubes, and membranes [2]. Facile integration of these materials into miniaturized analysis systems may also be readily achieved by taking advantage of selective *in situ* photopolymerization of the materials within optically transparent capillaries or microfluidic channels [12]. Furthermore, the immobilization of bioaffinity ligands, such as proteins, on their porous surfaces can enable macroporous polymers with to selectively enrich targeted biomolecules through stable and specific interactions [3–5,7,13,14], allowing these materials to serve as efficient stationary supports for a range of bioaffinity chromatography and biosensing platforms such as flow-through immunosensors [13,14].

Here we extend the concept of macroporous polymer-enabled biosensing to a new format consisting of functionalized macroporous methacrylate microspheres with excellent size uniformity. The microspheres are synthesized using a microfluidic co-flow emulsion technique to achieve large populations with exceptionally low polydispersity. Compared to established macroporous polymer formats, the tunable microspheres are suitable for use across a host of analytical applications or platforms, such as free-floating microbead sensors suspended in bulk solutions and multiplexed arrays of discrete sensor elements integrated within planar microfluidic devices. Here the microspheres are explored as discrete antibody-functionalized microscale immunosensor elements, or immunobeads. Solid non-porous immunobeads are routinely employed for a variety of analytical applications in the biological and medical sciences. Magnetic immunobeads have long been used in cell separation processes [9,15], and multiplexed immunobead assays employing readout techniques such as optical detection [16], flow cytometry [17], or agglutination [18] have been widely commercialized [19–22]. The macroporous immunobeads presented here represent an attractive alternative to traditional immunobeads which typically consist of solid silica or polymer particles. Compared to these established immunobeads, the macroporous microspheres offer significantly enhanced surface/volume ratios, using a facile fabrication process yielding nearly monodisperse populations of particles that offer access to simple immobilization methods for anchoring biomolecules on their surfaces.

* Corresponding author. Tel.: +1 301 405 8125.
** Corresponding author. Tel.: +1 301 405 8164.
E-mail addresses: sraghava@umd.edu (S.R. Raghavan), ddev@umd.edu (D.L. DeVoe).

0032-3861/$ – see front matter © 2012 Elsevier Ltd. All rights reserved.
http://dx.doi.org/10.1016/j.polymer.2012.09.059

Continuous-flow microfluidic fabrication of macroporous polymer microbeads is described, and preparation of the full immunobeads is demonstrated by selectively immobilizing anti-IgG antibodies on the surface of synthesized macroporous microspheres, followed by direct immunoassay characterization using fluorescein-labeled IgG as a target analyte. An efficient covalent anchoring method is described to significantly reduce background fluorescence and ensure high detection sensitivity. The resulting immunobeads reveal detection limits in the picomolar concentration range. The advantages of the macroporous structures are demonstrated through direct comparison to control samples of solid non-porous microbeads, revealing nearly order-of-magnitude improvement in detection limits for the macroporous immunobeads.

2. Experimental

Glycidyl methacrylate (GMA), 2,2-dimethoxy-2-phenyl-acetophenone (DMPA), decyl alcohol (DA), polyvinyl alcohol (PVA, 30K MW), Triton X-100, ethylenediamine (EDA), N-gamma-maleimido-butyryloxy-succinimide (GMBS), bovine serum albumin (BSA), phosphate buffer (PBS), and fluorescein isothiocyanate (FITC)-labeled rabbit IgG (MW ~140 kDa) were purchased from Sigma–Aldrich. Goat anti-rabbit IgG, methanol, acetone, and toluene were obtained from Thermo Fisher Scientific. The ethoxylated-trimethylolpropane-triacrylate (SR454) tri-vinyl acrylate crosslinker was received as a free sample from Sartomer.

The microfluidic co-flow tubing device used in all experiments (Fig. 1) was assembled from glass capillaries and microbore PTFE tubing in a manner similar to previous designs [23,24]. The inner glass capillary (VitroCom) was selected with dimensions of 50 μm ID and 80 μm OD, and the outer translucent PTFE tubing (Cole–Parmer) was chosen with an ID of 100 μm. The inner glass capillary, cleaved at a length of 5 cm, was first connected to one end of a 2.5 cm length of 250 μm ID and 750 μm OD Tygon tubing (Cole–Parmer). The other end of the Tygon tubing was inserted into a 10 μL plastic pipette tip with the end cut off. The open capillary end was positioned within the modified pipette top with a ~2 cm length outside the tip head. After inserting another Tygon tubing segment into the tail of the pipette for convenient introduction of the continuous phase, the tail was sealed with epoxy. At the pipette tip, the glass capillary was inserted into the PTFE tubing, and the tip of the pipette was sealed with Dow Corning 3140 silicone adhesive.

For the preparation of macroporous microspheres, the dispersed phase (36 wt% GMA, 24 wt% SR454, 39 wt% DA, 1 wt% DMPA) and the continuous phase (3 wt% PVA and 1% wt Triton X-100 in water) were injected separately by two syringe pumps (PHD 2000, Harvard Apparatus). Solid non-porous microspheres for control comparison were produced in the absence of the DA porogen, using a dispersed phase mixture consisting of 59 wt% GMA, 39.4 wt% SR454, and 1.6 wt% DMPA under the same setting-up conditions for macroporous microspheres preparation. Droplets were UV-cured *in-situ* while traveling along the tubing with a total UV exposure dose of 18 mW/cm^2. The stabilized microspheres were collected in a glass vial and exposed to an additional 15 min UV step at the same dose for full polymerization. After curing, the microspheres were thoroughly rinsed with methanol, acetone, toluene, acetone and DI water in sequence, and re-dispersed into 1× PBS buffer for storage. Imaging of pore morphology was performed by freezing collections of microspheres in liquid nitrogen, and cleavage the beads by a scalpel to expose the interior pores. Image analysis was performed using ImageJ software.

The microsphere surfaces were functionalized with bioactive proteins (anti-IgG) through two separate processing routes, namely glutaraldehyde and GMBS immobilization. In the glutaraldehyde route, the microspheres were immersed in a dilute solution of EDA in DI water (80% v/v) at 50 °C for 2 h, followed by rinsing with DI water and suspension in 10 wt% aqueous glutaraldehyde in 1× PBS buffer at room temperature (RT) for 3 h. In the GMBS route, the microspheres were immersed into 2.5 M CYS solution at RT for 2 h, followed by thorough rinsing with 20% v/v methanol in DI water and resuspension in 2 mM GMBS in ethanol for 2 h at RT following our previous protocol for continuous monolith functionalization [13]. After surface activation, the microspheres were fully washed by 1× PBS buffer and subsequently treated with goat anti-rabbit IgG antibody diluted in 1× PBS to a concentration of 50 μg/mL overnight at 4 °C. Immediately prior to testing, the microspheres were washed again with a solution of 2 mg/mL BSA in 1× PBS to block unreacted surface sites and reduce unwanted non-specific binding. FITC-labeled rabbit IgG (antigen) solutions with

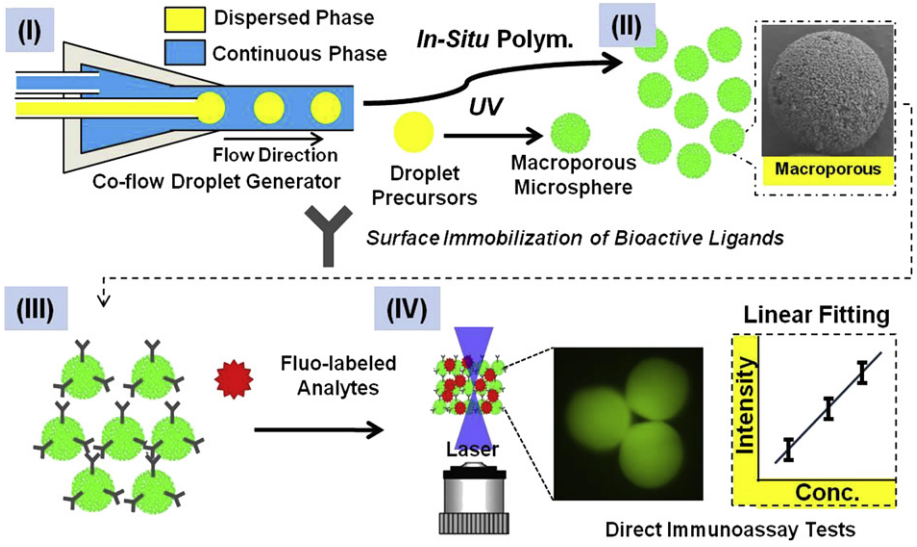

Fig. 1. Schematic of the macroporous microsphere synthesis and surface modification process: (I) microfluidic generation of droplet precursors in a co-flow droplet generator, with the dispersed phase composed of monomer GMA, crosslinker SR454, porogen DA, and photoinitiator DMPA sheared into discrete droplets by a continuous phase comprising an aqueous solution with surfactants. (II) UV photopolymerization of the droplet precursors for the formation of stable macroporous microspheres; (III) immobilization of capture antibody on the pore surfaces converts the microspheres into active immunobeads. (IV) Direct immunoassay test of immunobeads using fluorescent labeled antigen.

concentrations ascending from 2 ng/mL to 20 μg/mL were prepared in a buffer solution containing 2 mg/mL BSA in 1× PBS. The microspheres were incubated with 0.1 mL antigen solution in a glass vial for 30 min, followed by a final PBS rinse and in-solution optical detection.

Fluorescent measurements for immunoassay tests were performed on a Nikon TE-2000S inverted epi-fluorescence microscope. An excitation wavelength within the range of 465–495 nm was selected using a B-2E/C blue filter to detect the monolith-bound antigens. Scanning electron microscopy was performed on an Hitachi SU-70 SEM to characterize the macroporous structure of the microspheres, following ~20 nm gold sputter coating for improved surface contrast.

3. Results and discussion

3.1. Macroporous microsphere synthesis

Microfluidic synthesis of droplets has proven to be a highly effective method for the production of microparticles with unprecedented control over size, shape, and functional properties. While a range of microfluidic-based droplet preparation methods have been reported [23], all of these techniques involve the emulsification of one flow (dispersed phase) into a second immiscible flow (continuous phase) to create a stream of monodisperse droplets. For the production of solid polymer particles using this approach, the dispersed phase may consist of reactive monomers or oligomers, and these liquid droplet precursors can be subsequently be converted into solid microparticles by inducing physical or chemical crosslinking [25]. The size of the produced microparticles may be systematically adjusted in the range of a few micrometers to hundreds of micrometers by selecting appropriate microchanel dimensions and droplet formation topologies, fluid viscosities, and continuous/dispersed phase flow rate ratios [23,25]. Recently, the construction of microfluidic devices from glass capillary and plastic tubing has been used for droplet production as a simpler and more accessible alternative to traditional planar chip fabrication methods [23]. In the present work, a microfluidic tubing device comprising a co-flow droplet generator integrated with a downstream region for *in situ* UV polymerization was employed. A schematic of the system is shown in Fig. 1. The co-flow droplet generator consists of two separate capillaries assembled inside a modified pipette tip, where the outer diameter of the inner capillary was slightly smaller than the inner diameter of the outside capillary, allowing the inner capillary to fit into the microbore of the outer capillary with a defined circumferential gap to form a simple co-flow microfluidic device. The oil-based dispersed phase, comprised of a precursor mixture of monomer, crosslinker, porogen and photoinitiator, was injected through the inner capillary in the same direction of the aqueous continuous phase flowing through the outer capillary. A surface-active polymer (PVA) and surfactant (Triton X-100) were also added in the continuous phase for improved stability during droplet generation. At the tip of the inner capillary where the two immiscible flows meet, uniform droplets formed as a result of the interfacial tension and the shearing force imposed by the continuous phase [26]. The droplet volume can be tuned over a range of approximately 70–100 μm by adjusting the relative flow rates of each fluid stream, with the upper limit dictated by the inner diameter of the sheath flow capillary. In the present work we prepared microspheres with a mean diameter of 77 μm formed at dispersed and continuous flow rates of 2 μl/min and 30 μl/min, respectively. Size uniformity of the polymer microsphere under these conditions was excellent, with a standard deviation of 2.0 μm (2.6% relative standard deviation) measured by optical characterization over a sample size of 100 microspheres.

Following droplet generation, a downstream UV-curing zone was used to convert the fluid droplets into polymerized microspheres using a long transparent tube positioned beneath a UV light source. Upon UV exposure, the droplet precursor was converted into stable solidified microparticles as the *in situ* polymerization process proceeded. This process was monitored directly by observing the change in appearance of droplets from clear to semi-opaque. The opacity arises due to the formation of porous matrix resulting from dynamic phase separation of the acrylate polymer in the presence of the DA porogen. While the monomers are soluble in DA, the polymer is not [1]. In the process, the polymer phase-separates into submicrometer particles that aggregate to form a solid, connected network within the volume with the interstices filled with DA. A typical UV exposure time of 30 s, defined by the total flow rate and tubing length, was found to be sufficient to partially polymerize the droplets and stabilize their shape. The resulting microspheres were collected in a glass vial pre-filled with the continuous phase solution (Fig. 1). To ensure full conversion of the monomers, an additional 15 min UV exposure was performed following off-chip collection. Subsequently, the DA porogen and remaining unreacted reagents were washed from the microparticles by sequential rinses in methanol, acetone, and toluene.

In addition, non-porous microparticles were also prepared using the same procedure and experimental system, except that no porogen was added into the monomer mixture. These non-porous microparticles were used as control samples to evaluate signal enhancement for the macroporous immunobeads. No significant size variation between macroporous microspheres (77 μm) and non-porous microparticles (75 μm) was observed under the same preparation conditions for each case.

Fig. 2a and d show optical micrographs of the macroporous and non-porous microspheres produced using this technique. In each image, populations of both microbeads present well-arranged close-packed hexagonal patterns, confirming the nearly monodisperse nature of the resulting microspheres. Electron microscopy reveals that the microspheres prepared in the presence of porogen exhibit the expected co-continuous, macroporous texture, with fused clusters of sub-micrometer polymeric globules (Fig. 2b and c) and inter-connected flow through-pores that enable high permeability. In contrast, the solid microspheres formed in the absence of porogen do not exhibit any macroporosity. Just as with continuous monolithic stationary phase materials used in chromatography, the macroporosity of these microspheres, as well as the relative ratio of the skeletal structure and through pores, can be adjusted by varying synthesis parameters such as the relative concentrations of the monomer, crosslinker, and porogen [27–29]. The formation of a non-porous layer at the outer surface of the microspheres can be avoided by appropriate selection and proportion of porogens and surfactants [30].

Uniform porosity was also observed throughout the entire volume of the macroporous microspheres, as revealed by SEM imaging of a cleaved microparticle in Fig. 3a. The mean diameter of the macroporous microspheres was essentially identical to that of the non-porous control particles (Fig. 3b), indicating that phase separation between the polymer and porogen does not result in significant loss of porogen to the surrounding continuous phase for the conditions used in this work.

The morphological properties of the macroporous beads were determined by image analysis of high resolution SEMs taken from cleaved microspheres. The bead matrix was observed to be formed of individual GMA particles with a mean diameter of 600 nm, arranged in random clusters ranging from linear chains of individual particles to larger fused groups with total volumes corresponding to up to approximately 12 particles. Pore dimensions were assessed by measuring the largest circle circumscribed by the

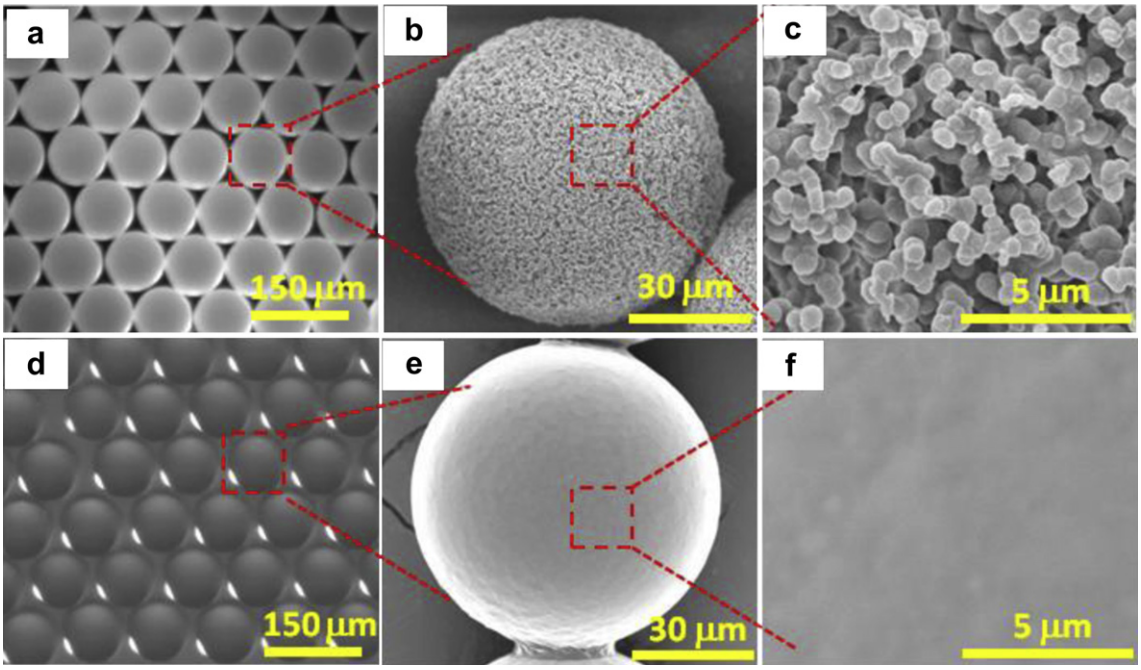

Fig. 2. (a) Optical micrograph of monodisperse macroporous microspheres prepared from the precursor recipe with monomer GMA, crosslinker SR454 and porogen DA. (b) Electron micrograph of a single microbead revealing its macroporous structure. (c) Magnified view of the porous morphology. (d) Optical microscope image of solid non-porous microbeads without the addition of porogen DA during preparation. (e) Electron micrograph of a non-porous microbead. (f) Magnified view of a solid bead surface revealing the lack of macroporosity.

surrounding polymer within a given plane of the beads, yielding a measured value of 1.6 ± 0.6 μm. Overall porosity was found to range between 44 and 50%, with no significant variation through the bead radius for any of the parameters.

The synthesis of various porous microparticles has previously been investigated using droplet microfluidics [31–36], with porous structures most commonly formed from heterogenous double emulsions that serve as templates to form voids and cavities within the final polymer spheres. In this approach, the dispersed phase is first emulsified with smaller inversed inert microemulsions that do not participate in the polymerization process. After droplet formation and polymerization, internal voids are formed by aggressive washing or evaporation to remove these inert microemulsions. The voids generated by these double emulsion methods are typically isolated, not interconnected as a result of their closed-cell morphologies, and would not benefit much for rapid molecular diffusion and transportation. In contrast, the structure of the macroporous microparticles synthesized through phase separation consists of extensively interconnected pores exhibiting an open-cell morphology. For analytical applications, this feature offers multiple pathways for rapid transport of analytes with low hydrodynamic resistance for efficient convection, and short diffusive length scales for rapid analyte/surface interactions.

Macroporous microspheres synthesized by phase separation have previously been demonstrated in work by Kumacheva et al. [28] in which the relationship between monomer composition and particle morphology was investigated. Here we describe a modified approach to the microfluidic synthesis of macroporous methacrylate microspheres that offers several advantages over prior methods, and further demonstrate an effective path to surface modification of the resulting porous microspheres to anchor bioactive species, enabling their use as discrete immunosensors. A unique feature of our synthesis route is the use of trivinyl crosslinking of SR454 to achieve large pore dimensions and enhance efficient convective transport of probe and analyte molecules through the monolith matrix [13,14]. Moreover, we note that unlike

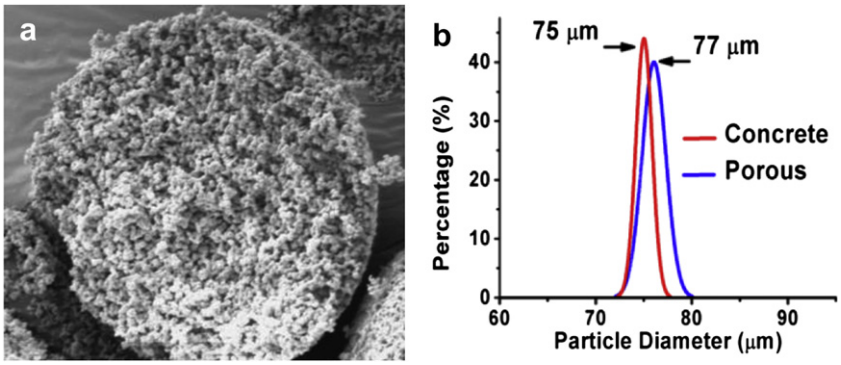

Fig. 3. (a) SEM image of a cleaved macroporous microspheres revealing uniform porosity throughout the particle volume. (b) Size distributions of both macroporous microspheres and solid non-porous microparticles showing excellent size uniformity. Data was obtained with a sample size of 100 microbeads in each case.

the previous use of phthalate plasticizers as porogens [28], which have recently raised wide environmental concern [37], here we have adopted decyl alcohol as a much safer alcohol-based solvent as the porogen while still achieving excellent control over the resulting pore dimensions. An additional unique aspect of the platform used for macroporous microsphere synthesis is its simplicity. All components are commercially available and readily assembled without any need for complicated or costly microfabrication equipment as commonly required in conventional microfluidic droplet synthesis methods [23,38,39]. The tubing method provides a simple route to the production of microfluidic devices supporting co-flow droplet generation that is accessible to labs and researchers without advanced microfabrication facilities or experience, with the use of a fluoropolymer as the outer tubing material making the platform suitable for either oil-in-water or water-in-oil emulsion systems [40].

3.2. Immunobead functionalization

A number of established routes are available to append desired surface functionalities on the macroporous polymer substrates, such as copolymerization of functional monomers, grafting functional side chains from surface reactive sites, or chemical modification of reactive functional groups. In the latter approach, various types of bioactive ligands, including proteins, enzymes, and carbohydrates have been covalently immobilized onto macroporous polymer substrates for use as stationary phase materials in affinity chromatography [4,7]. Here we adopt a similar strategy for immunobead production, with the use of GMA as the macroporous polymer offering several routes to simple and facile surface functionalization [3,4,7]. The pendant epoxide group of the polyGMA repeat unit can be easily reacted with primary amine/thiol groups of suitable crosslinkers and biomolecules through a specific nucleophilic epoxy ring-opening reaction [7]. Using this approach, the content of accessible epoxide groups on the macroporous matrix can be roughly estimated by comparing the ratio of GMA/SR454 added during preparation (60:40 by weight in the present work), and should be stoichiometrically excessive for subsequent surface modification steps. Svec and co-workers studied the heterogenous polymerization of GMA suspensions in aqueous continuous phase at the same 60 %wt feed amount and found that the GMA fraction in the polymerized product is in the range of 45%–60% [8]. In addition, a variety of linking methods for epoxide-presenting surfaces are readily available, such as direct epoxy anchoring [41], Schiff base reaction [3], and glutaraldehyde crosslinking [4,42].

As an initial study, we used glutaraldehyde, a dialdehyde crosslinker, to covalently immobilize goat anti-rabbit IgG on the surface of GMA macroporous microspheres. The GMA surface epoxides were first reacted with EDA, and then treated with glutaraldehyde through a robust aldehyde–amine reaction (Fig. 4a). One of the two aldehyde groups in a glutaraldehyde molecule first reacted with the amine group of EDA on the macroporous polymer surface, leaving the remaining aldehyde group on the other end of the glutaraldehyde free and active. The remaining free aldehyde was then reacted with the IgG primary amines to immobilize the antibodies on the polymer surface [4]. Since applications of functionalized macroporous materials have mainly been limited as monolithic stationary phases in separations or solid phases for extraction applications [2,6], evaluation of their optical performance, such as the background fluorescence induced during probe grafting, has generally been neglected in previous studies. However, in order to support analytical platforms where fluorescent optical readout is desirable, the impact of background fluorescence becomes an important consideration when selecting

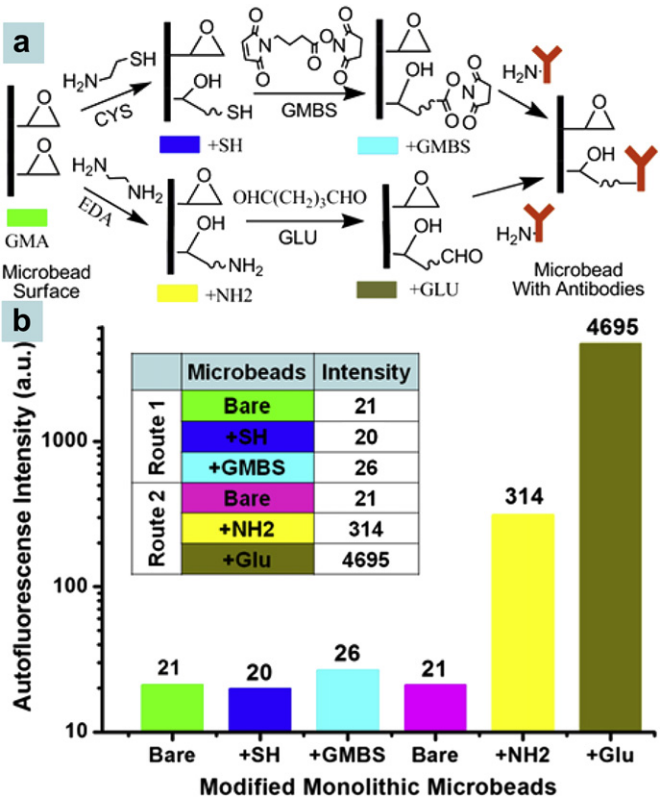

Fig. 4. (a) Schematic illustration of the GMBS and glutaraldehyde routes for immobilization of antibody on the monolith surface. (b) Auto-fluorescence measurements after each modification step reveals that the GMBS route reduces background fluorescence compared to the glutaraldehyde route by over 2 logs.

the appropriate grafting method. The glutaraldehyde anchoring method was found to suffer from significant enhancement in background fluorescence, with a 20 times increase following the initial ethylenediamine treatment, and a 300 times increase after glutaraldehyde modification. This behavior, which has been previously observed when fixing tissue specimens with glutaraldehyde [43], severely degrades the achievable fluorescence detection limits for immunobeads functionalized using this method. Another disadvantage of the glutaraldehyde route is that unsaturated imines formed during amine-aldehyde binding are susceptible to later hydrolysis under aqueous environments, thus requiring an additional stabilization step such as cyanoborohydride treatment [4].

As an alternative, we explored the use of GMBS as a heterobifunctional protein crosslinker to achieve efficient surface immobilization of antibodies on the porous GMA monolith surface. In this procedure, a thiol group is first introduced to the monolith through reaction between the epoxide group and cysteamine, followed by grafting of a GMBS molecule to the newly-formed thiol through reaction with the GMBS maleimido terminus [13], as depicted in Fig. 4a. The succinimidyl ester on the other side of GMBS is then used to bind directly with the primary amine of a target protein, namely goat anti-rabbit IgG antibody in the current study. We note that thiol groups exposed during the cysteamine reaction can themselves react with surface epoxides, thereby reducing the efficiency of GMBS anchoring on the thiol-presenting GMA surface, and alternative reaction routes capable of avoiding this path would be desirable to enhance GMBS density. Unlike the case of glutaraldehyde crosslinking, no increase in background fluorescence was observed when applying the GMBS anchoring route for antibody

immobilization on the macroporous microspheres (Fig. 4b). Moreover, the hetero-bifunctional GMBS crosslinker does not self-couple to large reactive biopolymers such as proteins and peptides, an issue with the homo-bifunctional glutaraldehyde route which could deactivate their biological functionalities. Similarly, the two termini of the glutaraldehyde molecule can react with two epoxide groups on the polymer surface, decreasing the density of available sites for protein immobilization [13].

3.3. Immunobead performance

To evaluate the performance of the GMA-based macroporous microspheres functionalized with GMBS-immobilized antibodies, a direct immunoassay test was performed using anti-IgG as a capture ligand for fluorescently-labeled rabbit IgG as a target antigen. Because unreacted thiols remaining on the GMA surface following antibody attachment present sites for non-specific proteins interactions through exposed cysteine residues, the fabricated immunobeads were incubated with BSA as a blocking agent before use to minimize non-specific binding. The use of BSA as a blocker was chosen since this approach is routinely used in ELISA and Western blot assays for clinical diagnosis and immunology studies. During the immunoassay test, anti-IgG functionalized macroporous microspheres were immersed into solutions of FITC-labeled IgG at concentrations ranging from 2 ng/mL to 200 μg/mL and incubated at room temperature for 30 min. After incubation, the microspheres were rinsed thoroughly in DI water to remove possible unbound antibodies. The resulting fluorescence intensity as a function of antibody concentration is shown in Fig. 5. The results reveal a nearly linear relation between emitted intensity and antibody concentration over a 5 log range, with a detection limit of approximately ~2 ng/mL (~14 pM) defined by a minimum signal-to-noise ratio of $S/N = 3$.

To investigate the impact of microsphere macroporosity on antigen capture, a control set of non-porous microbeads was prepared from a prepolymer solution lacking the addition of porogen (Fig. 2d–f). The non-porous microbeads were functionalized with anti-IgG using the same conditions employed for the macroporous microspheres. As depicted in Fig. 5, the fluorescence intensity of the solid, non-porous microspheres is significantly lower than the macroporous microspheres at each antibody concentration, with increasing disparity between the results at lower concentration levels. The significant difference on immunoassay performance between the two samples is attributed to the co-continuous, macroporous texture, which not only provides additional accessible surface area for the immobilization to achieve higher density of antibodies on the microsphere surface, but also encourages more efficient antibody–antigen interactions by a combination of steric entrapment and shortened diffusion lengths within the macroporous matrix.

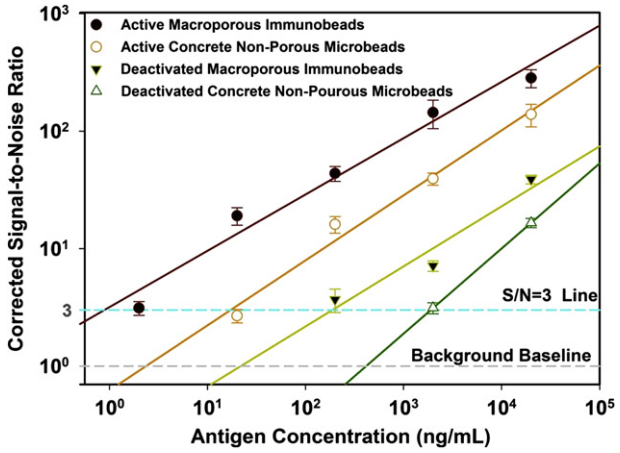

Fig. 5. Performance of anti-IgG functionalized immunobeads at different FITC-IgG concentrations. Control samples with deactivated anti-IgG on both macroporous microspheres and non-porous microbeads were also prepared to assess differences between specific and non-specific binding. Error bars reflect the standard deviation of fluorescence measurements performed from 10 individual immunobeads.

Quantitative comparison of specific and non-specific interactions was also performed through a parallel IgG dilution study. Identical surface modification and antibody immobilization procedures were used to functionalize both macroporous and non-porous microbeads, after which the antibodies on the polymer surfaces were deactivated by additional exposure to 70 °C for 1 h. Exposure to evaluated temperature denatures the F_{ab} fragments [44], resulting in irreversible aggregation of adjacent surface-bound antibodies and disrupting their biological functionality. Both the active and deactivated immunobeads retain the similar surface properties, but with different levels of bioactivity for specific antigen–antibody binding. Compared to active immunobeads, the deactivated microsphere exhibit a 1–2 log decrease in antibody capture for both the porous and non-porous cases, demonstrating that the majority of the fluorescence signal for the functional microparticles is due to specific interactions with surface-bound antigens as desired.

In the experiments presented here, diffusion serves as the dominant mechanism for transport of analyte through the porous beads during incubation with antigen in a static vial. For applications involving the use of fabricated microspheres in flow-through immunosensors, we note that the macroporous structure can provide a further benefit by allowing pressure-driven perfusion through the porous matrix for more rapid and efficient analyte/surface interactions. This phenomenon was recently investigated for the case of porous agarose bead sensors with sub-micrometer pore dimensions [45], and was previously explored for the case of dual-porosity beads for chromatographic applications [46,47]. For laminar Poiseuille flow through a tube, fluid flow velocity scales with the square of the tube diameter, and thus the perfusion velocity through the immunobead pores (u_p) relative to the interstitial flow (u_o) can be modeled as $u_p = (d_p^2/d_o^2)u_o$, where d_p and d_o are the hydraulic diameters of the pores and interstitial voids between immunobeads, respectively. For the case of close-packed immunobeads, the hydraulic diameter may be approximated as the diameter of the largest sphere that can fit through the narrowest opening between the immunobeads. From geometric analysis for the 77 μm diameter close-packed beads, the interstitial hydraulic diameter is estimated to be 12 μm, whereas the average hydraulic diameter of the pores is 1.6 μm. Thus the velocity of flow through the bead pores is expected to be approximately 1% of the interstitial flow velocity. While perfusion represents only a small portion of the overall flow, the use of high total flow rates can generate significant convective transport through the beads at a higher rate than diffusion alone.

4. Conclusions

A discrete immunosensor technology based on macroporous polymer immunobeads formed by a phase separation process has been developed. The microspheres were synthesized from precursor mixtures using a robust, continuous-flow, and high-throughput capillary co-flow platform with excellent control over size uniformity. Multiple routes for crosslinking antibodies to the porous polymer surface were evaluated toward their impact on optical properties of the functionalized microbeads, with GMBS

crosslinking identified as an efficient method yielding low autofluorescence.

Bioactive proteins were successfully anchored on the surface of the monolithic particles, enabling their use as versatile immunobeads suitable for a wide range of biosensing and bioassay applications. The combination of facile microfluidic synthesis, low polydispersity, excellent macroporosity with uniform and repeatable pore morphology, and straightforward route to biofunctionalization yielding low autofluorescence offers unique advantages toward the use of the immunobeads as discrete miniaturized biosensor elements, affinity supports for solid-phase extraction, catalyst carriers, and other applications where high surface area can enhance interactions between analytes in solution and microsphere-anchored biomolecules. The immunobeads were successfully evaluated through a direct immunoassay experiment using fluorescent readout, revealing a linear response over 5 logs of antigen concentration and a detection limit in the ng/mL range. While this work has focused on static immersion of the sensor elements in antigen solution, the macroporous immunobeads can provide further benefits in flow-through immunosensor applications, where interstitial perfusion through the porous matrix results in rapid convective transport coupled with short diffusion length scales for improved transport of analyte molecules to the polymer surface.

Acknowledgments

Funding from the UMD Center for Energetic Concepts Development and from DARPA is gratefully acknowledged. We thank the Maryland NanoCenter for access to facilities for SEM imaging.

References

[1] Okay O. Progress in Polymer Science 2000;25(6):711–79.
[2] Svec F. Journal of Separation Science 2004;27(10–11):747–66.
[3] Jiang T, Mallik R, Hage DS. Analytical Chemistry 2005;77(8):2362–72.
[4] Mallik R, Hage DS. Journal of Separation Science 2006;29(12):1686–704.
[5] Potter OG, Hilder EF. Journal of Separation Science 2008;31(11):1881–906.
[6] Svec F. Journal of Chromatography A 2010;1217(6):902–24.
[7] Tetala KKR, van Beek TA. Journal of Separation Science 2010;33(3):422–38.
[8] Svec F, Hradil J, Coupek J, Kalal J. Angewandte Makromolekulare Chemie 1975; 48:135–43.
[9] Hardingham JE, Kotasek D, Farmer B, Butler RN, Mi JX, Sage RE, et al. Cancer Research 1993;53(15):3455–8.
[10] Peters EC, Petro M, Svec F, Frechet JMJ. Analytical Chemistry 1998;70(11): 2288–95.
[11] Vázquez M, Paull B. Analytica Chimica Acta 2010;668(2):100–13.
[12] Nischang I, Brueggemann O, Svec F. Analytical and Bioanalytical Chemistry 2010;397(3):953–60.
[13] Liu JK, Chen CF, Chang CW, DeVoe DL. Biosensors & Bioelectronics 2010;26(1): 182–8.
[14] Liu JK, White I, DeVoe DL. Analytical Chemistry 2011;83(6):2119–24.
[15] Rye PD, Hoifodt HK, Overli GE, Fodstad O. American Journal of Pathology 1997;150(1):99–106.
[16] Morgan E, Varro R, Sepulveda H, Ember JA, Apgar J, Wilson J, et al. Clinical Immunology 2004;110(3):252–66.
[17] Vignali DAA. Journal of Immunological Methods 2000;243(1–2):243–55.
[18] Elshal MF, McCoy JP. Methods 2006;38(4):317–23.
[19] Pollema CH, Ruzicka J, Christian GD, Lernmark A. Analytical Chemistry 1992; 64(13):1356–61.
[20] Evans ML, Chan PJ, Patton WC, King A. Fertil Steril 1998;70(2):344–9.
[21] Arellano-Garcia ME, Hu S, Wang J, Henson B, Zhou H, Chia D, et al. Oral Diseases 2008;14(8):705–12.
[22] Dekking EH, van der Velden VH, Varro R, Wai H, Bottcher S, Kneba M, et al. Leukemia 2012;26(9):1976–85.
[23] Shah RK, Shum HC, Rowat AC, Lee D, Agresti JJ, Utada AS, et al. Materials Today 2008;11(4):18–27.
[24] Hwang H, Kim S-H, Yang S-M. Lab on a Chip 2011;11(1):87–92.
[25] Il Park J, Saffari A, Kumar S, Gunther A, Kumacheva E. Annual Review of Materials Research 2010;40:415–43.
[26] Jeong WJ, Kim JY, Choo J, Lee EK, Han CS, Beebe DJ, et al. Langmuir 2005;21(9): 3738–41.
[27] Wang QC, Hosoya K, Svec F, Frechet JMJ. Analytical Chemistry 1992;64(11): 1232–8.
[28] Dubinsky S, Zhang H, Nie ZH, Gourevich I, Voicu D, Deetz M, et al. Macromolecules 2008;41(10):3555–61.
[29] Beiler B, Vincze A, Svec F, Safrany A. Polymer 2007;48(11):3033–40.
[30] Dubinsky S, Park JI, Gourevich I, Chan C, Deetz M, Kumacheva E. Macromolecules 2009;42(6):1990–4.
[31] Zhang H, Cooper AI. Soft Matter 2005;1(2):107–13.
[32] Partap S, Rehman I, Jones JR, Darr JA. Advanced Materials 2006;18(4):501–4.
[33] Zhou WQ, Gu TY, Su ZG, Ma GH. Polymer 2007;48(7):1981–8.
[34] Zhou WQ, Gu TY, Su ZG, Ma GH. European Polymer Journal 2007;43(10): 4493–502.
[35] Choi S-W, Zhang Y, Xia Y. Advanced Functional Materials 2009;19(18): 2943–9.
[36] Fernández-Trillo F, van Hest JCM, Thies JC, Michon T, Weberskirch R, Cameron NR. Advanced Materials 2009;21(1):55–9.
[37] Yen T-H, Lin-Tan D-T, Lin J-L. Journal of the Formosan Medical Association 2011;110(11):671–84.
[38] Xia YN, Whitesides GM. Angewandte Chemie-International Edition 1998; 37(5):551–75.
[39] Becker H, Gartner C. Electrophoresis 2000;21(1):12–26.
[40] Nightingale AM, Krishnadasan SH, Berhanu D, Niu X, Drury C, McIntyre R, et al. Lab on a Chip 2011;11(7):1221–7.
[41] Mallik R, Jiang T, Hage DS. Analytical Chemistry 2004;76(23):7013–22.
[42] Petro M, Svec F, Fréchet JMJ. Biotechnology and Bioengineering 1996;49(4): 355–63.
[43] Collins JS, Goldsmith TH. Journal of Histochemistry & Cytochemistry 1981; 29(3):411–4.
[44] Vermeer AWP, Norde W. Biophysical Journal 2000;78(1):394–404.
[45] Chou J, Lennart A, Wong J, Ali MF, Floriano PN, Christodoulides N, et al. Analytical Chemistry 2012;84(5):2569–75.
[46] Li Q, Zhu J, Daugulis AJ, Hsu CC, Goosen MFA. Biomaterials Artificial Cells and Immobilization Biotechnology 1993;21(3):391–8.
[47] Gustavsson PE, Axelsson A, Larsson PO. Journal of Chromatography A 1998; 795(2):199–210.